

Advances in Low Voltage Electron Microscopy from Imaging to Analytical Perspective

P. Woo*, M. Ohno*, S. Takeuchi**, R. Gauvin***, N. Brodusch***, and H. Demers***

* Hitachi High-Technologies Canada, Inc. 89 Galaxy Blvd., Toronto, Canada.

** Hitachi High-Technologies Corporation., 882 Ichige, Hitachinaka, Ibaraki, Japan.

*** McGill University, Department of Materials Engineering, Montreal, Canada.

Scanning Electron Microscope (SEM) is currently an inevitable tool in the field of science due to its superior resolution and analytical capabilities compared to an optical microscope. Low voltage electron microscopy (i.e: $V_{acc} < 5kV$) often provides a more detailed image and also helps to reduce the effects of charging on poorly conducting samples. However, the imaging resolution of electron microscope, operated at low accelerating voltage, is always worse than its higher energy counterpart. This is mainly the result of the decrease in gun brightness and the increase in various aberrations when electron optics operate at a lower kV. With the improvements in electron emission sources (i.e: from thermionic W-hairpin to Cold field-emission) and objective lens design (i.e: from simple asymmetric pin-hole lens to immersion type In-lens), sub-nanometer resolution can now be obtained at low accelerating voltages. With the introduction of the snorkel lens, providing a strong magnetic field that can travel outside the pole-piece, and allows the electron beam to be continuously focused and extends down to the specimen. This yields a low lens aberration value similar to In-lens systems and it also allows the possibility to accommodate large specimens as with a pin-hole type lens system. Moreover, by utilizing the same magnetic field generated by the snorkel lens, this design enables the capture of secondary electrons traveling inside of the pole-piece. In comparisons to a conventional lower detector, this through-the-lens, or upper detector provides unique advantages in further improving resolution by filtering out SE3 (SEs with a higher energy spread) and BSEs (higher beam interaction volume). With the recent introduction of in-lens top detector a further improvement in the collection efficiency of accelerated SE signals, with low landing voltage, allows significantly improved topmost surface imaging with enhanced elemental contrast[1].

Conventional cold-field emitter provides superior advantages in high-resolution imaging due to its superior brightness, lowest energy spread, and extended source lifetime among all electron sources. However, it also has a few weaknesses such as insufficient maximum probe current ($< 30nA$) and beam stability ($\Delta 3-5\%/hr$) for some applications. The cold-field emitter has lower maximum probe current compared to Schottky field emitter and tungsten hairpin due to its much smaller source size ($< 5nm$, $15-30nm$ and $30-100\mu m$, respectively for CFE, SFE and W-hairpin). A smaller source size would mean less demagnification in the electron optics in order to achieve a small enough probe diameter for high resolution imaging. Cold field emission also requires the emitter surface to be atomically clean. As a result, it generally requires an operation vacuum level of $< 10^{-8}Pa$ and a “flashing” procedure prior to operation by heating the tip for a very short time to a temperature of $\sim 2400K$. Afterward, a monolayer of gas molecules will form around tip, and the emission will stabilize and remain relatively constant for 8-12hrs until whiskers are formed on the surface due to aggregation of adsorbates. At this time the tip will require flashing to return to the original state. Generally speaking, the beam current stability during the stable period is measured to be around $4\%/hr$, in contrast to $\sim 0.5\%/hr$ for SFE.

Very recently, a newly designed cold field emitter system was developed by utilizing an additional Non-Evaporative Getter (NEG) pump installed around the emitter area[2]. With the new NEG pump, an ultimate vacuum of $\sim 10^{-10}Pa$ can be achieved, resulting in a much slower deposition of adsorbates around the tip. Since the emitter always operates in a “clean” state, source brightness is significantly improved with a three-fold increase in probe current and beam current stability of $\sim 0.8\%/hr$.

Energy dispersive x-ray spectroscopy (EDX) has always been one of the most popular accessories installed on an SEM. Traditionally the detector is mounted on a side port, at an angle between 30-40°, relative to the sample surface. Depending on the size of the x-ray detector, the solid angle for a typical SEM ranges from 0.00625 to 0.05sr for a single detector setup. Recently, a novel four quadrant x-ray detector has been commercialized. The detector is placed flat between sample and the microscope pole piece[3]. This setup provides a solid angle of ~1.1sr offering an order of magnitude higher x-ray counts compared to a conventional setup.

The combination of the new CFEG, SE detectors and flat quad x-ray detector open a new gateway to low voltage imaging and microanalysis. For example, figure 1 showed the SEM micrographs of the cathode material used in lithium-ion battery. These images were obtained under beam deceleration conditions at a landing voltage of 200V. The image obtained with the top detector clearly reveals the active material is covered by a light element residue. On the other hand, with a conventional upper detector, material contrast cannot be seen and phase identification would be difficult based upon looking at the surface morphology. Figure 2 showed the same material analyzed using the flat quad x-ray detector. Here, it is confirmed that the active material consisted of Cobalt and Nickel rich Oxides and the residue is identified as Fluorine on a carbon rich matrix. Note that the x-ray analysis was carried at an acceleration voltage of 2kV with only 4 minutes of acquisition time.

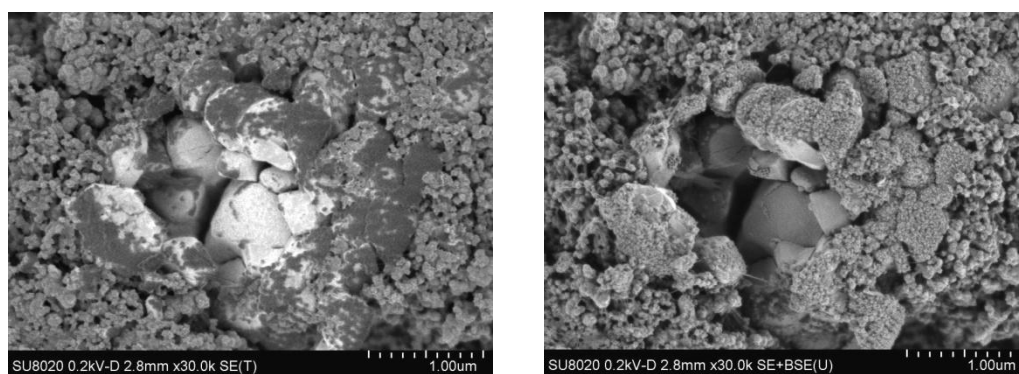


FIG. 1 – Combinations of In-lens top detector and low landing voltage helped in revealing organic residue found in top-most surface of Li-ion battery.

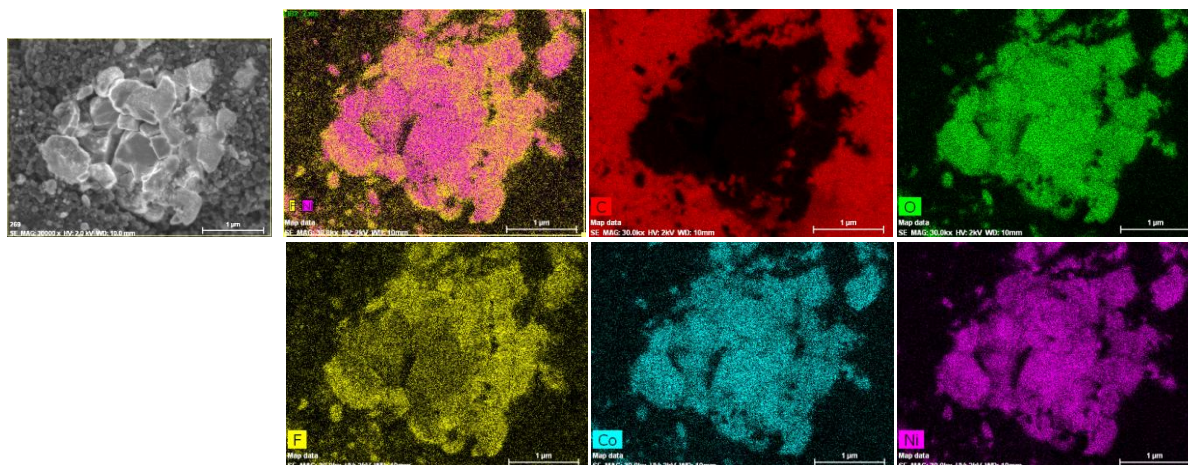


FIG 2. – X-ray microanalysis obtained from the same area as shown in figure 1.

References

- [1] Takeuchi S., Miyaki A., Muto A., Okada S., Hatano M., and Ito S., *Microscopy and Microanalysis*, 16-S2 (2010) 616
- [2] Kasuya K., Kimura M., Katagiri S., and Ohshima T., *Microscopy and Microanalysis*, 16-S2 (2010) 6
- [3] Terborg R., Kappel A., and Salge T., *Microscopy and Microanalysis*, 16-S2 (2010) 1302